J. Fluid Mech. (2003), *vol.* 492, *pp.* 289–302.
DOI: 10.1017/S0022112003005676 Printed in the United Kingdom

Instabilities of the Stewartson layer Part 1. The dependence on the sign of *Ro*

By RAINER HOLLERBACH†

Department of Aerodynamics and Fluid Mechanics, Brandenburg Technical University, 03013 Cottbus, Germany

(Received 16 August 2002 and in revised form 16 May 2003)

We consider the fluid flow in a spherical shell in rapid overall rotation, with additionally a differential rotation imposed on the inner sphere. The basic state consists of the axisymmetric Stewartson shear layer situated on the tangent cylinder, the cylinder parallel to the axis of rotation and just touching the inner sphere. In this work we consider the non-axisymmetric instabilities that arise when the differential rotation becomes sufficiently large. We find that the sign of the differential rotation, that is, whether the inner sphere is rotating slightly faster or slightly slower than the outer sphere, is crucial, with positive differential rotations yielding a progression to higher wavenumbers m as the overall rotation rate increases, but negative differential rotations yielding $m = 1$ over almost the entire range of rotation rates. This difference is particularly intriguing, as it has been seen before in one closely related experimental study, but not in another. A prior asymptotic analysis also suggested there should be no difference. We therefore try to understand what subtle features of the flow structures and/or geometries should cause this difference in results. We show that the geometry is the critical feature, with the height along the axis of rotation changing abruptly across the tangent cylinder. We are not able to identify why this should make such a difference, and why only for negative differential rotations. We suggest instead additional experiments and asymptotics to further clarify this point.

1. Introduction

Among the fundamental problems in classical fluid dynamics are the possible instabilities of free shear layers, with a history dating back to von Helmholtz (1868), Lord Kelvin (1871) and Lord Rayleigh (1880), and continuing to this day (e.g. Chomaz *et al.* 1988; Solomon, Holloway & Swinney 1993; van de Konijnenberg *et al.* 1999). Such shear flow instabilities are of interest not only from an abstract fluid-dynamical point of view; they are also relevant in meteorology (Kuo 1973), oceanography (Talley 1983), astrophysics (Sumathi & Raghavachar 1993), and many other areas.

In this work we will consider the instabilities of the Stewartson layer, a particularly simple shear layer that exists in rapidly rotating systems. The instabilities of this layer have previously been studied experimentally (Hide & Titman 1967; Niino & Misawa 1984; Früh & Read 1999), and these results are largely understood in terms of Busse's (1968) asymptotic analysis. There is, however, one key discrepancy between the experiments of Hide & Titman and Früh & Read that is not explained by the

† Permanent address: Department of Mathematics, University of Glasgow, Glasgow G12 8QW, UK.

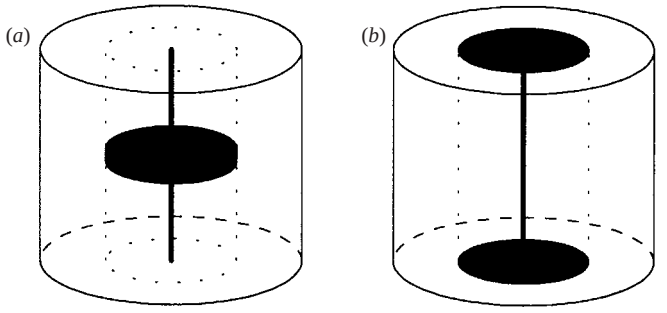

FIGURE 1. Sketches of the experimental setups of (*a*) Hide & Titman, and (*b*) Früh & Read. The disks indicated in black are given a differential rotation $\Delta\Omega$ in addition to the overall rotation Ω. The dotted lines denote the tangent cylinder on which the basic Stewartson layer forms.

theory. The purpose of this work is to explore the origin of this discrepancy, by presenting a direct numerical solution of a closely related problem.

The Stewartson layer is generated by imposing a small differential rotation on part of a system in rapid overall rotation. Figure 1 shows sketches of the two experimental configurations adopted by Hide & Titman and Früh & Read. In both cases a cylindrical container rapidly rotates about the vertical axis. Hide & Titman (subsequently referred to as HT) then impose a differential rotation on a small disk immersed in the middle of the tank; Früh & Read (subsequently referred to as FR) impose a differential rotation on two small disks embedded in the top and bottom boundaries of the tank. In both cases the resulting flow pattern consists primarily of a shear layer on the tangent cylinder, the cylinder circumscribing the disk(s) and parallel to the axis of rotation. Outside the tangent cylinder the fluid rotates at a rate Ω, the overall rotation of the container; inside the tangent cylinder it rotates at a rate $\Omega + \Delta\Omega/2$ in the HT setup and $\Omega + \Delta\Omega$ in the FR setup, where in both cases $\Delta\Omega$ is the differential rotation of the disk(s). (That is, the fluid everywhere rotates at a rate intermediate between its upper and lower boundaries.) The detailed structure of the shear layer which then resolves this jump in angular velocity across the tangent cylinder was derived by Stewartson (1957), and consists of two nested layers of outer thickness $E^{1/4}$ and inner thickness $E^{1/3}$, where the Ekman number E is an inverse measure of the overall rotation rate Ω.

Stewartson's analysis only applies in the limit of infinitesimally small $\Delta\Omega$, in which inertia can be neglected by linearizing about $\boldsymbol{U} = 0$ (in the rotating system). However, for increasingly large $\Delta\Omega$, for which inertia can no longer be neglected, it seems likely that eventually some sort of instability will set in, and indeed that is what the experiments reveal. For sufficiently large $\Delta\Omega$ the initially axisymmetric Stewartson layer becomes unstable, and adopts a wavy, non-axisymmetric structure instead.

Although the experiments thus agree that instabilities will eventually set in, they disagree on quite fundamental aspects of these instabilities. In particular, FR find that the sign of $\Delta\Omega$, that is, whether their two disks are rotating slightly faster or slower than the tank, makes virtually no difference for $|\Delta\Omega/\Omega|$ as large as ~ 0.5; in both cases the azimuthal wavenumber of the most unstable non-axisymmetric mode gradually increases with decreasing Ekman number. (As one might expect, since the preferred azimuthal lengthscale of the instability might be expected to become shorter and shorter as the radial lengthscale of the underlying shear layer becomes shorter and

shorter.) In contrast, HT find that this sign is crucial, with the azimuthal wavenumber increasing if their one disk is rotating slightly faster, but remaining constant at $m = 1$ if it is rotating slightly slower. (Niino & Misawa only considered the case of positive $\Delta\Omega$, so their results are less relevant in this context.)

This discrepancy between HT and FR in the case of negative $\Delta\Omega$ is particularly intriguing as Busse (1968) had predicted there should be no difference between positive and negative $\Delta\Omega$ (by reducing the governing equations to a barotropic, quasi-geostrophic form in which the sign of $\Delta\Omega$ does not enter at all). There must thus be some subtle difference in the geometries or flow patterns between figures 1(*a*) and 1(*b*), which makes Busse's analysis more applicable to 1(*b*) than to 1(*a*). There are a number of obvious differences between 1(*a*) and 1(*b*) (which we will consider in detail below), but it is not immediately obvious which of these should matter and why, and why only for negative $\Delta\Omega$. Until we can answer these questions, we cannot say that we fully understand the results of either HT or FR.

In an attempt to address at least some of these questions I here present a direct numerical solution of a closely related problem, namely the instabilities of the Stewartson layer in spherical rather than cylindrical geometry. If one considers a rapidly rotating spherical shell, and imposes a small differential rotation on the inner sphere, a Stewartson layer will again be induced on the tangent cylinder. The detailed structure of this layer was obtained by Stewartson (1966), and is almost identical to the previous structure, again consisting of nested layers of outer thickness $E^{1/4}$ and inner thickness $E^{1/3}$, but now also containing an intermediate thickness $E^{2/7}$. The Stewartson layer in spherical geometry has also been reproduced numerically by Hollerbach (1994) down to $E = 10^{-5}$, and by Dormy, Cardin & Jault (1998) down to $E = 10^{-7}$, with good agreement with the asymptotic analysis in both cases.

Given that the Stewartson layers in spherical and cylindrical geometries are so similar, one might expect that the two problems would also give rise to similar instabilities. This is indeed the case; the instabilities we obtain here are almost identical to the HT ones, and in particular exhibit the same difference between positive and negative $\Delta\Omega$. We therefore conduct various numerical experiments to elucidate the origin of this difference. We show that it is due to the variation in height of fluid columns parallel to the axis of rotation, with this height changing abruptly across the tangent cylinder both here and in figure 1(*a*), but not in 1(*b*). We are not able definitely to identify why this should make such a difference, and why only for negative $\Delta\Omega$. Instead, we suggest further experiments in which this geometrical effect is more systematically studied, as well as further asymptotics of some of these new configurations.

2. Equations

Scaling length by the gap width $(r_o - r_i)$, time by the inverse rotation rate Ω^{-1}, and $\boldsymbol{U}$ by $\Delta\Omega\,(r_o - r_i)$, the Navier-Stokes equation in the rotating frame becomes

$$\frac{\partial \boldsymbol{U}}{\partial t} + Ro\,\boldsymbol{U}\cdot\nabla\boldsymbol{U} + 2\hat{\boldsymbol{e}}_z \times \boldsymbol{U} = -\nabla p + E\nabla^2\boldsymbol{U}, \tag{1}$$

where the Ekman number

$$E \equiv \frac{\nu}{\Omega(r_o - r_i)^2} \tag{2}$$

is thus an inverse measure of the overall rotation rate Ω, and the Rossby number

$$Ro \equiv \Delta\Omega/\Omega \tag{3}$$

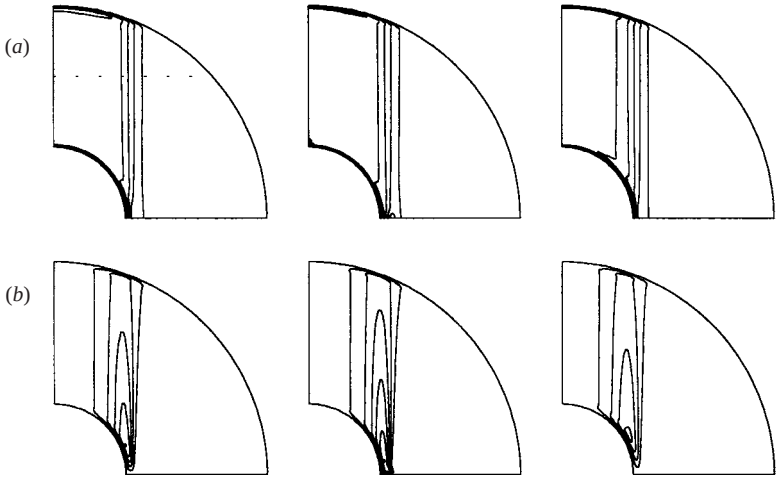

FIGURE 2. (*a*) Contours of the angular velocity, with a contour interval of 0.1. (*b*) Streamlines of the associated meridional circulation, with a contour interval of 2×10^{-4}. From left to right $Ro = 0$, 0.5 and -0.5, and $E = 10^{-4}$. The angular velocity is symmetric about the equator, the meridional circulation anti-symmetric (that is, counter-clockwise in the upper hemisphere, clockwise in the lower). Finally, the dotted line in the left panel of (*a*) indicates the plane $z = 1$; in figure 3 we show profiles of the angular velocity as a function of the cylindrical radius along this line.

is the relative differential rotation rate. In the experiments E typically ranges between 10^{-2} and 10^{-5}, and $|Ro|$ between 0 and $O(1)$. Very conveniently this is also the range that is numerically accessible. The boundary conditions associated with (1) are

$$\left.\begin{aligned} \boldsymbol{U} &= r \sin\theta\, \hat{\boldsymbol{e}}_\phi \quad \text{at} \quad r = r_i, \\ \boldsymbol{U} &= 0 \qquad\qquad \text{at} \quad r = r_o, \end{aligned}\right\} \tag{4}$$

where we fix the inner and outer radii at $r_i = 1/2$ and $r_o = 3/2$.

The numerical code we use to solve these equations (along with the incompressibility condition $\nabla \cdot \boldsymbol{U} = 0$) is described by Hollerbach (2000). Two slightly different versions of this code were used. We begin by considering purely axisymmetric solutions, thereby computing the basic states whose instabilities we want to consider. These results are presented in the next section. In §§4 and 5 we then linearize about these basic states and compute the stability of single non-axisymmetric modes at a time.

3. Axisymmetric solutions

Figure 2 shows the equilibrated, steady-state solutions at $E = 10^{-4}$ and $Ro = 0$, 0.5 and -0.5. The shear layer on the tangent cylinder is clearly visible, with the fluid at rest outside, and rotating at a rate intermediate between the inner and outer spheres inside. The Ekman layers of thickness $E^{1/2}$ at the inner and outer boundaries are also visible. A slight thickening of the inner Ekman layers toward the equator can just be seen, where the $E^{1/2}$ scaling breaks down entirely, and is replaced by an $E^{2/5}$ scaling (Stewartson 1966, see also Hollerbach 1994 and Dormy *et al.* 1998).

In addition to these various structures shown by the angular velocity, there is also a secondary meridional circulation, consisting of a flow from the outer to the inner Ekman layer inside the tangent cylinder, with the return flow in a narrow jet on the tangent cylinder. This flow is very weak compared with the azimuthal shear, only

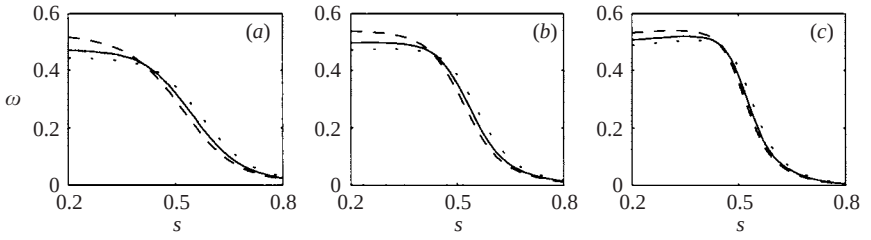

FIGURE 3. The angular velocity ω as a function of the cylindrical radius s, at $z=1$ for (*a*) $E=10^{-3.5}$, (*b*) $E=10^{-4}$, (*c*) $E=10^{-4.5}$. In addition to $Ro=0$, indicated by the solid line, in (*a*) $Ro=\pm 0.7$ is shown, in (*b*) $Ro=\pm 0.5$ and in (*c*) $Ro=\pm 0.3$. Positive Ro are shown dotted, negative dashed.

$O(E^{1/2})$. (Incidentally, we note also that with our scaling for $\boldsymbol{U}$, the dimensional and non-dimensional flows are in opposite directions for $\Delta\Omega<0$. That is, while the non-dimensional circulation shown here is counter-clockwise for all Ro, the real, dimensional circulation would be clockwise for $Ro<0$.)

Turning to the Ro-dependence, we note that there is remarkably little; the solutions for $Ro=\pm 0.5$ — already a substantial differential rotation — look very similar to the solution for $Ro=0$, corresponding to an infinitesimal differential rotation (the limit considered by Stewartson, Hollerbach 1994 and Dormy *et al.* 1998). For even larger positive Ro the solutions do change significantly, with purely axisymmetric instabilities developing, and the solutions becoming time-dependent. Since we will find in the next section that $Ro=0.5$ is already unstable to non-axisymmetric instabilities, the existence of these axisymmetric instabilities is of little interest. In the parameter ranges of interest the basic states always remained steady-state. They also remained equatorially symmetric, as indicated in figure 2. Perturbations of the opposite symmetry were introduced, but decayed away in every case. Finally, figure 3 shows detailed profiles of $\omega(s)$ across the layer. We see both how it becomes thinner and thinner for increasingly small E, and the comparatively minor effect that variations in Ro have.

4. Non-axisymmetric instabilities

Having obtained these axisymmetric basic states $\boldsymbol{U}_0$, we next linearize (1) about them to obtain

$$\frac{\partial \boldsymbol{u}}{\partial t}+Ro\,(\boldsymbol{u}\cdot\nabla\boldsymbol{U}_0+\boldsymbol{U}_0\cdot\nabla\boldsymbol{u})+2\hat{\boldsymbol{e}}_z\times\boldsymbol{u}=-\nabla p+E\nabla^2\boldsymbol{u}. \tag{5}$$

We can therefore test the stability of $\boldsymbol{U}_0$ by time-stepping (5) (with homogeneous boundary conditions) until the dominant eigenmode emerges, and seeing whether it grows or decays. Conveniently, the problem continues to be two-dimensional, even though it is no longer axisymmetric, since the different non-axisymmetric modes decouple, and can therefore be tested separately. Because of the equatorial symmetry shown in figure 2, each m further decouples into two distinct symmetry classes that can again be tested separately. It was found though that only modes having the same symmetry as the basic state became unstable.

The procedure is therefore as follows. Fix E and Ro, and compute the axisymmetric basic state according to (1). Then time-step (5) for a given m (and symmetry class) until the dominant eigenmode emerges. If it grows/decays, decrease/increase Ro and

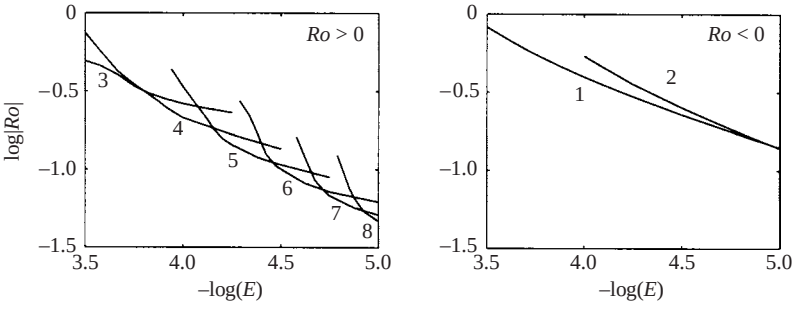

FIGURE 4. Ro_c versus E, for the different azimuthal wavenumbers indicated. Modes not shown ($m=1$ and 2 for $Ro>0$ and $m>2$ for $Ro<0$) may still be unstable, but are not the most unstable modes for any values of E.

repeat the whole procedure (including the calculation of $\boldsymbol{U}_0$) until one obtains Ro_c, the critical Rossby number where the instability just sets in. By repeating this procedure in turn for a range of Ekman numbers, one can map out Ro_c as a function of E, for any given value of m.

Figure 4 shows these results, for positive and negative Ro. The similarity with HT is striking; we also find that for positive Ro the most unstable azimuthal wavenumber increases with decreasing E, whereas for negative Ro it remains constant at $m=1$ over almost the entire range of E. For both positive and negative values Ro_c decreases with decreasing E (although it is perhaps worth noting that it decreases sufficiently slowly that the absolute, dimensional differential rotation $\Delta\Omega_c$ increases). This also is in agreement both with the experiments and with Busse's asymptotics; HT obtain $Ro_c \propto E^{0.6}$ (for both signs of Ro, curiously), FR obtain $Ro_c \propto E^{0.72}$ (again for both signs of Ro), Busse predicts $Ro_c \propto E^{0.75}$, and we here obtain $E^{0.65}$ for positive Ro, and $E^{0.45}$ for negative Ro.

5. Why are sgn(Ro) $=\pm1$ different?

Having obtained the same difference between positive and negative Ro as HT, we now consider its origin. First we should note that there is no *a priori* reason why the two cases should not be different; they are physically distinct states. Without the results of Busse and FR, therefore, we might accept that different states simply have different instabilities as well. Given their results though, we would like to understand why $\pm Ro$ are different in figure 1(a) and here, but not in figure 1(b) and Busse's asymptotics.

5.1. *Testing aspects of* $\boldsymbol{U}_0$

There are three aspects of $\boldsymbol{U}_0$ that we can test (and in the end eliminate) as possible causes of this difference. The first is that the nonlinearity in $\boldsymbol{U}_0$, that is, its dependence on Ro, is the cause. Given how weak this dependence is, it seems unlikely, but we can verify it easily by conducting the following numerical experiment: for $\boldsymbol{U}_0$ in (5), always use the $Ro=0$ basic state. That is, adjust Ro in (5), but fix it at zero in (1). Doing this, we obtain instability curves very similar to those in figure 4, proving that the nonlinearity in $\boldsymbol{U}_0$ has virtually no effect, and is certainly not the cause of the difference between positive and negative Ro.

The next aspect of $\boldsymbol{U}_0$ we consider is the meridional circulation. Given how weak this is, it again seems implausible that this would have any significant effect, but we

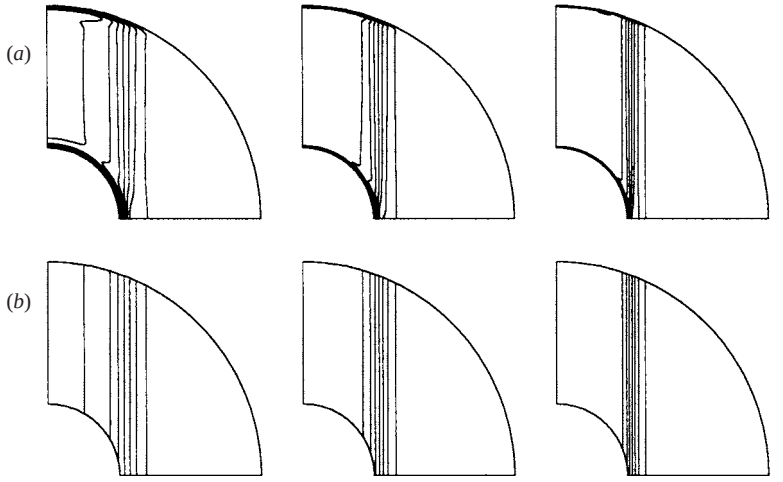

FIGURE 5. (*a*) Contours of the angular velocity, for $Ro = 0$ and, from left to right, $E = 10^{-3.5}$, 10^{-4} and $10^{-4.5}$; (*b*) shows how the Ekman layers have been removed, by extending to all z the previous profiles at $z = 1$. These are thus the basic states used in the computation of figure 6. The contour interval is 1/15 throughout.

can again verify this, by conducting a similar experiment, in which we simply delete the meridional circulation from $\boldsymbol{U}_0$ in (5) (And of course, having just verified that the slight *Ro*-dependence of the basic state does not make a difference, we could save time by always using the $Ro = 0$ basic states here as well.) Once again, we obtain instability curves very similar to those in figure 4.

The last aspect of $\boldsymbol{U}_0$ that we consider are the Ekman layers at the inner and outer boundaries in figure 2. We explore here whether the instabilities we see really are instabilities of the Stewartson layer, and not of the Ekman layers: after all, the jump in angular velocity across the Ekman layers is exactly the same as across the Stewartson layer, and they are even thinner, so the shear is greater. It is thus not obvious that the Stewartson layer will nevertheless become unstable first.

Returning to figure 1, we recall also that inside the tangent cylinder the angular velocity is $\Omega + \Delta\Omega/2$ in figure 1(*a*), but $\Omega + \Delta\Omega$ in 1(*b*). That is, figure 1(*a*) will have Ekman layers just like those here, whereas 1(*b*) will not. Furthermore, Busse did not include Ekman layers in the basic state whose stability he studied, but simply prescribed a shear profile without any z-dependence. That is, if these anomalous negative-*Ro* instabilities turned out to be instabilities of the Ekman layers rather than the Stewartson layer, that would certainly be consistent between the four sets of results: in HT and here there are both Ekman layers and anomalous negative-*Ro* instabilities, whereas in FR and Busse there are neither.

It is thus clear that of our three numerical experiments on $\boldsymbol{U}_0$, testing the influence of the Ekman layers is the most important. We therefore conduct an experiment similar to the above two, namely to delete the Ekman layers as well from $\boldsymbol{U}_0$ in (5). This is a little more involved than deleting the meridional circulation, but is ultimately still quite straightforward, with figure 5 showing the result. Figure 6 then shows the resulting instability curves, which we note are still much the same as in figure 4. Though plausible, this correlation between Ekman layers and these anomalous instabilities is not the explanation.

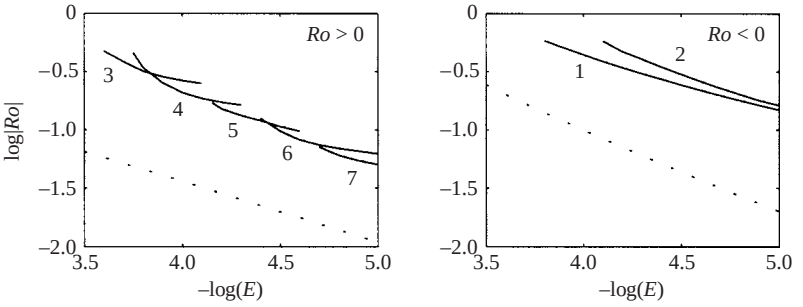

FIGURE 6. Ro_c versus E, for the different azimuthal wavenumbers indicated, with the nonlinearity, meridional circulation and Ekman layers all deleted in $\boldsymbol{U}_0$. The significance of the dotted lines will be explained in § 5.3.

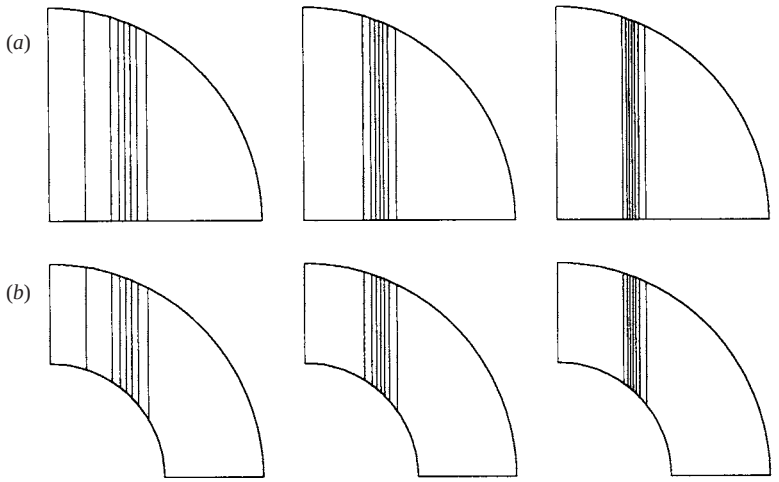

FIGURE 7. (*a*) How the shear profiles from figure 5 are extended into a full sphere, (*b*) how they are restricted to a shell with $r_i = 0.8$ (rather than the original 0.5).

5.2. *Influence of the geometry*

At this point the only remaining part of $\boldsymbol{U}_0$ is the z-independent shear shown in figure 5, and yet we still obtain this difference between positive and negative Ro, whereas – with virtually the same basic state – Busse and FR do not. We conclude therefore that the critical difference between figures 1(*a*) and 1(*b*) lies in the geometry itself, rather than in the resulting flows. Fortunately, we can vary the geometry as well, as shown in figure 7, in which the profiles in figure 5 are either extended into a full sphere, or restricted to a thinner shell than before. (Note also that even though these various checks on $\boldsymbol{U}_0$ all turned out negative, it was nevertheless important to do them first, as it would have been rather more difficult to extend the original $\boldsymbol{U}_0$ into a different geometry. Extending a z-independent basic state is trivial though.)

Figure 8 shows the resulting instability curves, which are (finally) different from figure 4. In both the full sphere and thin shell geometries, positive and negative Ro are much the same, with both now exhibiting a progression to higher and higher wavenumbers, as found by Busse and FR. In all four cases we also find that $Ro_c \propto E^{0.7}$, that is, in better agreement with FR and Busse than in figure 4.

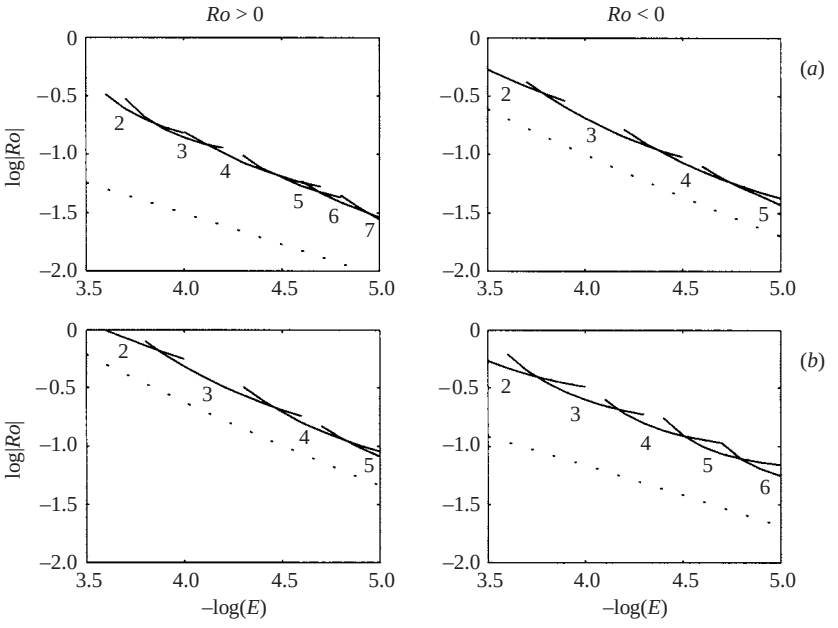

FIGURE 8. Ro_c versus E, for the different azimuthal wavenumbers indicated, with the (a, b) corresponding to the geometries and basic states shown in (a) and (b) of figure 7.

Having demonstrated that the geometry is the crucial factor, we now consider precisely what aspect of it causes the difference, and why. We begin by introducing the height along the z-axis, h, as a function of the cylindrical radius s. In the full sphere this height decreases on moving outward across the shear layer, whereas in the thin shell it increases. In contrast, in the original $r_i = 0.5$ shell it decreases in both directions away from the tangent cylinder, with $h' \to \infty$ just inside the tangent cylinder, due to the slope of the inner sphere becoming vertical there.

Turning next to HT, FR, and Busse, we note that HT also change h discontinuously across the tangent cylinder, due to the finite thickness of the disk (12.5 mm, compared to an Ekman layer thickness of 1–3 mm). In contrast, FR do not change h, and Busse also considered primarily this case. This leaves only the two cases in figures 7 and 8, where h' is either uniformly positive or uniformly negative across the shear layer. Busse considered these cases as well, and again concluded that the sign of Ro should not matter, in perfect agreement with what we obtain here.

The conclusion therefore seems quite clear: if h does not change, or changes gradually, then positive and negative Ro will be much the same, whereas if it changes abruptly, then negative Ro will be anomalous. We now consider various diagnostic quantities that might help in understanding why that is the case.

5.3. *Diagnostics*

First we consider the so-called potential vorticity

$$PV = \frac{2 + Ro(\nabla \times \boldsymbol{U}_0)_z}{h(s)}, \tag{6}$$

consisting of the total vorticity, including that due to the background rotation, divided by the height $h(s)$. The reason potential vorticity might be important is that for almost

z-independent flows such as here, it is conserved on fluid columns (in the inviscid limit, at least). See, for example, Salmon (1998) for this result (which corresponds physically to conservation of local angular momentum). If PV is to be conserved on fluid columns, a necessary condition for instability is presumably that $PV' = 0$ (assuming the instability involves fluid columns moving in and out in s, as non-axisymmetric instabilities necessarily do). With such an instability criterion, it is then not difficult to see why variations in h would matter, or why positive and negative Ro might be quite different. See, for example, Li & McClimans (2000) or Burns, Maslowe & Brown (2002) for two such stability calculations.

We should caution, though, that PV is an essentially inviscid concept, and therefore may not be directly applicable to a problem such as that considered here, where viscosity (in the form of the Ekman number) plays an essential role. For example, if h is constant, $PV' = 0$ when $Ro = 0$, which is indeed the correct $E = 0$ limit of FR and Busse's results, but is still not helpful in understanding the finite E results. Nevertheless, given how ubiquitous PV is in the geophysical fluid dynamics literature, and how it can explain $\pm Ro$ asymmetries in certain problems, it is worth considering if it can be correlated at least qualitatively with some of the results.

The dotted lines in figures 6 and 8 show the critical Rossby numbers at which the potential vorticity gradient first becomes 0 at some point, given the $\boldsymbol{U}_0$ profile at that Ekman number (and of course with $h(s)$ as appropriate for the given geometry). Turning to the simpler geometries in figure 8 first, we find that the results are certainly suggestive, with these critical Rossby numbers following much the same $E^{0.7}$ scaling as the critical Rossby numbers for the onset of instability. Indeed, this $PV' = 0$ criterion might even explain much of the variation in the overall level of the instability curves, that is, the constant multiplying the $E^{0.7}$. For $h'Ro > 0$ the instabilities consistently appear to set in at twice the $PV' = 0$ value; for $h'Ro < 0$ at three to four times.

Turning to the original figure 6 geometry, $Ro < 0$ is once again anomalous, in the sense that it is the only case where the slopes of the $PV' = 0$ and instability curves are quite different, suggesting that perhaps PV plays a role in all the other instabilities, but not in these. However, this conclusion is rather tentative at best; it would have been less so if, for example, the $PV' = 0$ curve had been above the instability curves in this one case. As it is, these potential vorticity diagnostics are inconclusive so far.

We therefore turn to our next set of diagnostics, the spatial structure of the instabilities, and where they extract their energy from the basic state, which apart from their intrinsic interest, could cast further light on the question of whether PV is relevant or not, since, if it is, the instabilities might be expected to be concentrated where PV' is small.

We begin by deriving the energy equation associated with (5). Taking the dot product of it with $\boldsymbol{u}$ and integrating over the shell, one obtains after a little algebra

$$\frac{\partial}{\partial t}\int \tfrac{1}{2}\boldsymbol{u}^2\,\mathrm{d}V = Ro\int \boldsymbol{U}_0\cdot((\nabla\times\boldsymbol{u})\times\boldsymbol{u})\,\mathrm{d}V - E\int|\nabla\times\boldsymbol{u}|^2\,\mathrm{d}V. \tag{7}$$

All other terms, such as $-\boldsymbol{u}\cdot\nabla p$, yield zero when integrated over the shell. That is, they may rearrange the energy, but neither create nor destroy it. There are a number of uses to which we may put (7). At Ro_c the two terms on the right must exactly balance one another (since then the instability is neither growing nor decaying), which they do, to within better than 1% (the same accuracy to which Ro_c was computed), thereby providing a reassuring check of the numerical implementation and resolution.

Beyond this global energy balance, however, it is useful to look at the detailed spatial structures of some of the terms in (7), for example $Ro\,\boldsymbol{U}_0\cdot[(\nabla\times\boldsymbol{u})\times\boldsymbol{u}]$ as a

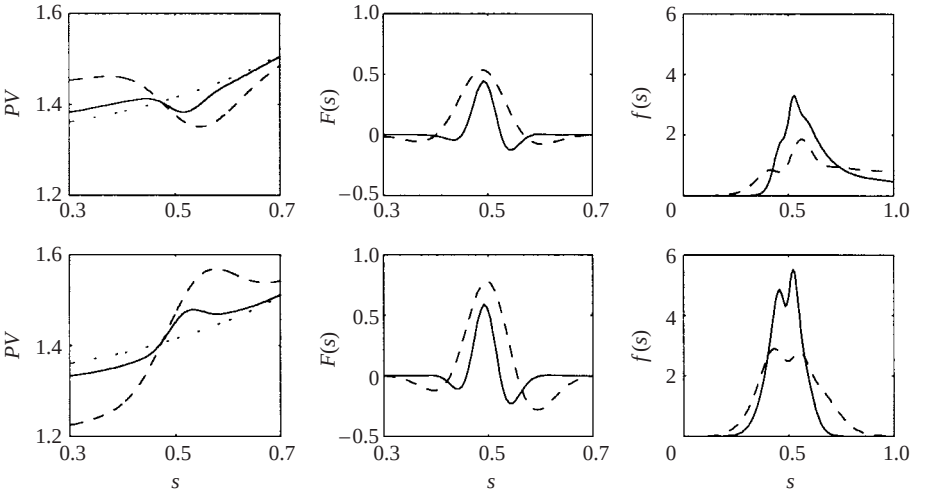

FIGURE 9. The three quantities PV, $F(s)$ and $f(s)$. Positive Ro for the top row, negative for the bottom. The solid lines in each panel are at $E = 10^{-5}$, the dashed lines at $E = 10^{-4}$. Finally, the dotted lines in the PV plots show the purely geometrical quantity $2/h(s)$ – from which one may deduce that this figure corresponds to the full sphere geometry.

function of (s, ϕ, z). The ϕ-dependence cannot be too complicated, since $\boldsymbol{u}$ consists of a single $\exp(im\phi)$ mode. The z-dependence is similarly straightforward; like $\boldsymbol{U}_0$, $\boldsymbol{u}$ turns out to be largely independent of z. We therefore focus on the s-dependence by defining

$$F(s) = Ro \int\int \boldsymbol{U}_0 \cdot ((\nabla \times \boldsymbol{u}) \times \boldsymbol{u})\, s \, \mathrm{d}\phi \, \mathrm{d}z \tag{8}$$

(that is, we include all of $\mathrm{d}V$ except the integration over s). We similarly define

$$f(s) = \int\int \tfrac{1}{2} \boldsymbol{u}^2 \, s \, \mathrm{d}\phi \, \mathrm{d}z \tag{9}$$

to study the localization in s of $\boldsymbol{u}$. (In both (8) and (9) $\boldsymbol{u}$ is normalized such that the total energy is unity, that is, $\int f(s)\, \mathrm{d}s = 1$.)

Figures 9–11 then show some of these diagnostics, for the three geometries $r_i = 0, 0.8$ and the original 0.5, and for positive and negative Ro in each case. Again considering the simpler geometries first, we note in figures 9 and 10 that – as expected – $F(s)$ is strongly concentrated on the shear layer at $s = 0.5$, and becomes increasingly concentrated as E is reduced. However, there is no tendency for the peak in F to coincide with regions of particularly small PV' (which would have meant slightly displacing F from $s = 0.5$). Similarly, $f(s)$ also peaks at $s = 0.5$, but again with no correlation with PV'. The other interesting point to note about f is how the $Ro > 0$ case in figure 9 and the $Ro < 0$ case in figure 10 both extend far beyond $s = 0.5$. That is, what little difference there is between positive and negative Ro is again correlated with the sign of h', just as in figure 8. (In the bottom right panel in figure 10 one can also note the influence of the new tangent cylinder at $r_i = 0.8$; the eigenmodes extend out to there, but then drop off very abruptly.)

Turning next to the original geometry, we note in figure 11 that yet again $Ro < 0$ is anomalous. For $Ro > 0$ functions F and f appear similar to some of the results in the simpler geometries. The potential vorticity is of course somewhat more complicated,

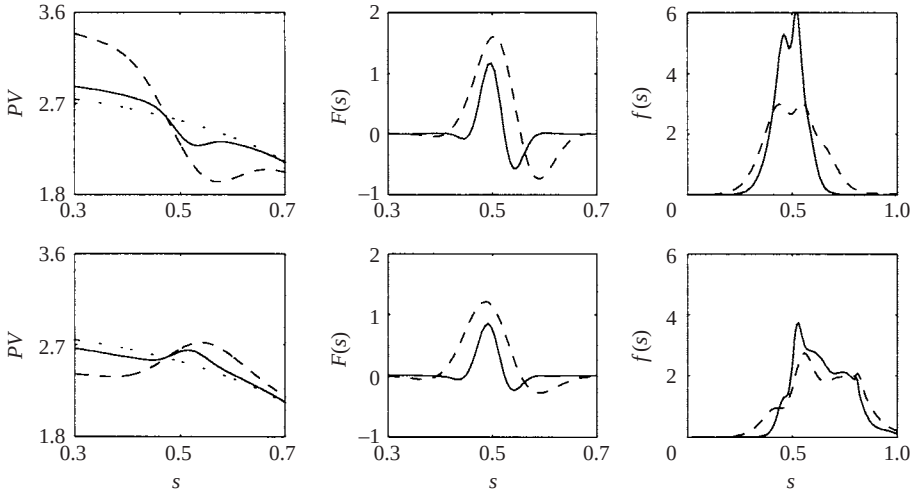

FIGURE 10. As in figure 9, but now for the $r_i = 0.8$ thin shell geometry.

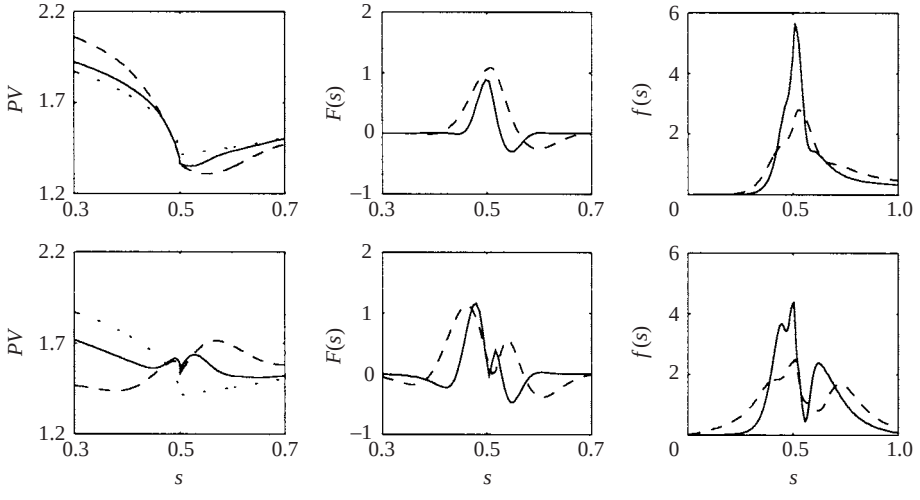

FIGURE 11. As in figure 9, but now for the original $r_i = 0.5$ geometry.

due to the presence of the vertical tangent as $s \to 0.5$ from below. Nevertheless, it is not very different from some of the earlier results; in particular, PV' is also negative just outside $s = 0.5$, resulting in a reasonably smooth curve. In contrast, for $Ro < 0$ all three panels look quite different from any of the other results; F and especially f both appear to have split into two distinct peaks, and PV exhibits a very sharp cusp at $s = 0.5$. It is tempting therefore to ascribe the origin of these anomalous negative Ro results to the presence of this cusp, but there is no rigorous justification.

Finally, we note also that in changing from $E = 10^{-4}$ to 10^{-5} in figures 9–11, the most unstable mode changes in all but the bottom row in figure 11 (see figures 6 and 8). However, the s-dependence is unaffected, merely more concentrated exactly as one would expect, but otherwise much the same even for different m.

6. Conclusion

In this work we have considered the instabilities of the Stewartson layer, and in particular their sgn(Ro) dependence. By conducting various numerical experiments we showed that this dependence is determined by the way in which the height $h(s)$ varies across the shear layer. If h does not change, or changes smoothly, then positive and negative Ro will be much the same, whereas if it changes abruptly $\pm Ro$ will be very different. This result that h' is the crucial factor then strongly suggests that PV is the underlying dynamically significant quantity. Unfortunately, the various potential vorticity diagnostics were perhaps suggestive, but ultimately inconclusive.

Additional experiments (real, not numerical) might help to further illuminate this problem, and the role that potential vorticity may play in it. First, HT's experiment should be repeated with disks of varying thickness, to study more systematically the effect that the resulting jump in h has. Next, one could add offsets to the top and bottom boundaries (in either the HT or FR setups) in such a way that h suddenly decreases rather than increases. Would $Ro > 0$ then be the anomalous case?

Another interesting possibility would be to adjust the boundaries in such a way that h itself does not change abruptly, but h' does, discontinuously switching from positive inside the tangent cylinder to negative outside. Would that be enough to make $Ro < 0$ anomalous, or is an abrupt change in h itself (that is, $h' \to \infty$) required? (This is something that we are not able to test here; by adjusting the geometry to remove the $h' \to \infty$ singularity, we automatically also ensure that it will be continuous, and of the same sign across the whole shear layer.) And if this experiment did yield anomalous results for $Ro < 0$, would discontinuously switching h' from negative inside to positive outside yield anomalous results for $Ro > 0$?

In parallel with these various experiments, the asymptotic analysis could be extended to some of them. Incorporating abrupt changes in h itself might prove rather difficult, but extending Busse's analysis to allow for an abrupt change in the sign of h' might be helpful, certainly if the experiments do yield anomalous results in these cases.

Another problem where an asymptotic analysis might prove revealing is a closely related magnetic one, in which a layer much like the Stewartson layer is generated by imposing a magnetic field rather than an overall rotation. The instabilities of this so-called parallel layer were obtained numerically by Hollerbach & Skinner (2001), and found to be very similar to the $Ro > 0$ results here. This similarity between the two problems, in terms of both the basic states and the instabilities, is reason enough to consider them side by side, but there is also one crucial difference between the two, namely that whereas here the sign of the differential rotation matters, in the magnetic problem the sign of the inner sphere's rotation (the only rotation present in that problem) does not. The magnetic problem contains an additional symmetry not present in (1), which ensures that the relative orientations of the magnetic field and the rotation do not enter.

Finally, returning to the Stewartson layer problem considered here, one might ask what happens to these instabilities in the supercritical regime. At what levels do they equilibrate, and how do they react back on the basic state? These issues will be addressed in a future paper, in which we will also make a direct comparison with experimental results (although at $r_i/r_o = 2/3$ rather than $1/3$, to match the Egbers & Rath (1995) apparatus).

I thank Bill Young for pointing out how to test the influence of geometry in § 5.2, and an anonymous referee for emphasizing the importance of potential vorticity. I

also thank the Alexander von Humboldt Foundation for supporting my sabbatical in Germany.

REFERENCES

Burns, A. G., Maslowe, S. A. & Brown, S. N. 2002 Barotropic instability of the Bickley jet at high Reynolds numbers. *Stud. Appl. Maths* **109**, 279–296.

Busse, F. H. 1968 Shear flow instabilities in rotating systems. *J. Fluid Mech.* **33**, 577–589.

Chomaz, J. M., Rabaud, M., Basdevant, C. & Couder, Y. 1988 Experimental and numerical investigation of a forced circular shear layer. *J. Fluid Mech.* **187**, 115–140.

Dormy, E., Cardin, P. & Jault, D. 1998 MHD flow in a slightly differentially rotating spherical shell, with conducting inner core, in a dipolar magnetic field. *Earth Planet. Sci. Lett.* **160**, 15–30.

Egbers, C. & Rath, H. J. 1995 The existence of Taylor vortices and wide-gap instabilities in spherical Couette flow. *Acta Mech.* **111**, 125–140.

Früh, W. G. & Read, P. L. 1999 Experiments on a barotropic rotating shear layer. Part 1. Instability and steady vortices. *J. Fluid Mech.* **383**, 143–173 (referred to herein as FR).

von Helmholtz, H. 1868 On discontinuous movements of fluids. *Phil. Mag.* **36**, 337–346.

Hide, R. & Titman, C. W. 1967 Detached shear layers in a rotating fluid. *J. Fluid Mech.* **29**, 39–60 (referred to herein as HT).

Hollerbach, R. 1994 Magnetohydrodynamic Ekman and Stewartson layers in a rotating spherical shell. *Proc. R. Soc. Lond.* A **444**, 333–346.

Hollerbach, R. 2000 A spectral solution of the magneto-convection equations in spherical geometry. *Intl J. Numer. Meth. Fluids* **32**, 773–797.

Hollerbach, R. & Skinner, S. 2001 Instabilities of magnetically induced shear layers and jets. *Proc. R. Soc. Lond.* A **457**, 785–802.

Kelvin, Lord 1871 Hydrokinematic solutions and observations. *Phil. Mag.* **42**, 362–377.

van de Konijnenberg, J. A., Nielsen, A. H., Rasmussen, J. J. & Stenum, B. 1999 Shear-flow instability in a rotating fluid. *J. Fluid Mech.* **387**, 177–204.

Kuo, H. L. 1973 Dynamics of quasigeostrophic flows and instability theory. *Adv. Appl. Mech.* **13**, 247–330.

Li, S. & McClimans, T. A. 2000 On the stability of barotropic prograde and retrograde jets along a bottom slope. *J. Geophys. Res.* **105**, 8847–8855.

Niino, H. & Misawa, N. 1984 An experimental and theoretical study of barotropic instability. *J. Atmos. Sci.* **41**, 1992–2011.

Rayleigh, Lord 1880 On the stability or instability of certain fluid motions. *Proc. Lond. Math. Soc.* **11**, 57–70.

Salmon, R. 1998 *Lectures on Geophysical Fluid Dynamics.* Oxford University Press.

Solomon, T. H., Holloway, W. J. & Swinney, H. L. 1993 Shear flow instabilities and Rossby waves in barotropic flow in a rotating annulus. *Phys. Fluids* **5**, 1971–1982.

Stewartson, K. 1957 On almost rigid rotations. *J. Fluid Mech.* **3**, 17–26.

Stewartson, K. 1966 On almost rigid rotations. Part 2. *J. Fluid Mech.* **26**, 131–144.

Sumathi, K. & Raghavachar, M. R. 1993 Shear flow instabilities in rotating systems. *Astrophys. Space Sci.* **199**, 89–104.

Talley, L. D. 1983 Radiating barotropic instability. *J. Phys. Oceanogr.* **13**, 972–987.